Optimal Scheduling of Home Energy Management System with Plug-in Electric

Vehicles Using Model Predictive Control

by

Yue Zhao

A Thesis Presented in Partial Fulfillment
of the Requirements for the Degree
Master of Science

Approved June 2018 by the
Graduate Supervisory Committee:

Yan Chen, Chair
Nathan Johnson
Qin Lei

ARIZONA STATE UNIVERSITY

August 2018

ABSTRACT

With the growing penetration of plug-in electric vehicles (PEVs), the impact of the PEV charging brought to the utility grid draws more and more attention. This thesis focused on the optimization of a home energy management system (HEMS) with the presence of PEVs. For a household microgrid with photovoltaic (PV) panels and PEVs, a HEMS using model predictive control (MPC) is designed to achieve the optimal PEV charging. Soft electric loads and an energy storage system (ESS) are also considered in the optimization of PEV charging in the MPC framework. The MPC is solved through mixed-integer linear programming (MILP) by considering the relationship of energy flows in the optimization problem. Through the simulation results, the performance of optimization results under various electricity price plans is evaluated. The influences of PV capacities on the optimization results of electricity cost are also discussed. Furthermore, the hardware development of a microgrid prototype is also described in this thesis.

ACKNOWLEDGMENT

TABLE OF CONTENTS

LIST OF TABLES

LIST OF FIGURES

LIST OF SYMBOLS

CHAPTER 1. INTRODUCTION

1.1 Background and Motivation

Along with the growing penetration of plug-in electric vehicles (PEVs) in the automobile market, including both plug-in hybrid electric vehicles and pure electric vehicles, the adoption and implementation of PEV charging from the utility grid initiates some new challenges. For example, the loads for charging a PEV with a charging power of 19kW at 80A and 240V, which is known as the AC level 2 charging standard, can be almost 20 times of that for supporting a typical North American home [1]. Furthermore, for places where multiple PEVs and relatively close charging schedules are involved, like PEV charging station in a parking lot, the problem of load imbalance could be severe and thus affect the distribution grid [2]. Therefore, the PEV charging strategy or smart charging needs to be systematically explored. Another motivation for studying this topic is that we would like to find a way to calculate an optimal solution on energy management strategy for the users.

1.2 Problem Statement

To address problems brought by PEV charging, different studies were conducted on different levels: smart grid oriented, aggregator oriented, and customer oriented [3]. Different methods have different optimization goals and control access, based on different scales of the controlled systems. Smart grid oriented PEV charging focuses on the control of power system on a large scale, especially on the stability and reliability of a smart grid. For example, voltage regulation and frequency regulation, as well as load flattening. In studies on smart grid oriented PEV charging, the economic benefits are usually not

considered as an optimization goal. Aggregator oriented is a perspective between the power system and single users. The aggregator can be local public facilities like parking lots or residential areas. It can be regarded as a local utility grid that is a piece of the large power grid, and connect it with the customer. The aggregator is responsible for the stability and reliability of the electricity, and also has the concern of economic benefits. Customer oriented control represents the users' interest, which is mainly cost minimization.

There are many scenarios that include PEV charging, and each has a different requirement. Thus, different system structures are designed. For example, for a parking lot for workplaces capable of PEV charging, the charging time often happens in the daytime. Thus the design of using PV generation without ESS is often proposed [4] [5]. The ESS is not needed because the charging curve matches the power generation curve of PV, which all reach its maximum at mid-day. Furthermore, the type of PEV charger varies, mainly can be divided into two types: DC charger and AC charger. DC charger means the charger is connected to DC bus, this type of design usually appears in charging infrastructures with large scales [6] [7], DC charger supports fast charging which is convenient for such scenarios. AC charger, however, often has less maximum available power for PEV charging, is used more in places where a DC bus is not present, especially in the household scenario.

In this study, a customer-oriented PEV charging optimization problem is discussed. Specifically, if the problem of PEV charging for every single node in a microgrid, namely a single household, is addressed and solved, it will also benefit the regional power grid. One promising method to reduce potentially negative influences on the utility grid with the

2
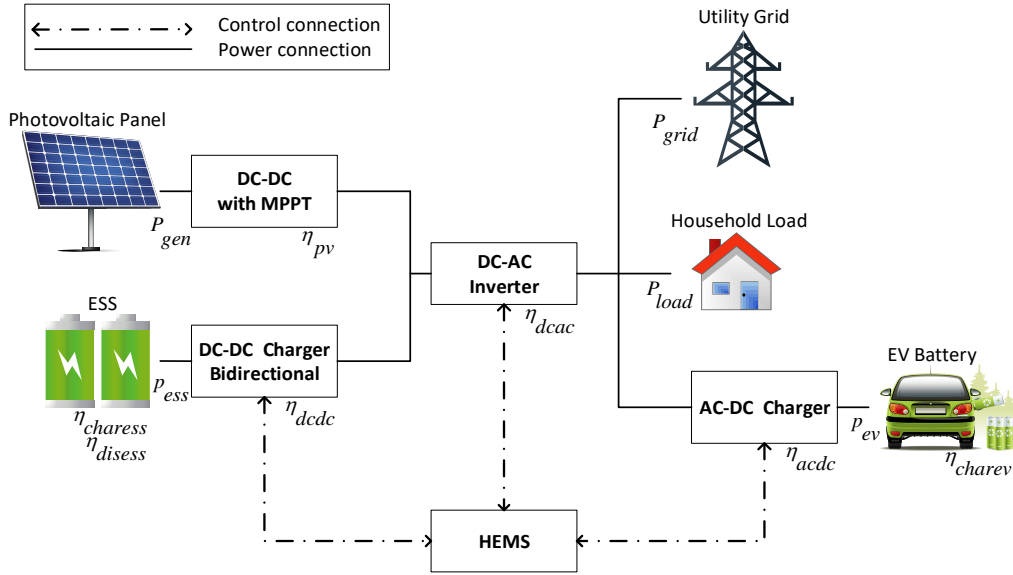
Figure 1. EMS diagram of a household microgrid with PEV.

PEV charging is to introduce renewable energy sources in the household microgrid. Among various renewable energy sources, photovoltaic (PV) panel module is one of the widely appropriate choices for the advantages of reduced purchase cost, environmental impact, and maintenance [4].

For most household applications, the pattern of load requirements typically does not match the generation curve of PV panels. Thus, more flexibility and capability to utilize and manage the generated energy is preferred. An energy storage system (ESS), like an industrial battery, is usually introduced in a household microgrid together with a home energy management system (HEMS) for this purpose. In some studies [1] [8] [9], batteries in PEVs were regarded as ESS with the function of vehicle-to-load (V2L) or vehicle-to-grid (V2G). However, for household applications, using PEV as ESS has several disadvantages. First, by allowing the battery of PEV charge energy back to the utility grid, the charger is required to be bi-directional, which is not yet fully developed in the market

and adds cost for initial investment. Second, if the vehicle is taken out of the household, the ESS is no longer available. When that occurs, the HEMS has no energy storage to utilize. Furthermore, if energy is drawn from the PEV before the PEV is driven out, it might leave the user with a less charged car. Third, enabling V2G or V2L means a more frequent and intensive use of EV battery, which degrades the battery health thus the longevity of the battery life will be shorter than expected. Whether V2G and V2L could bring economic benefits or not was not easy to justify considering PEV battery degradation effects [10]. Instead, adding an extra set of batteries as ESS designed explicitly for the energy storage purpose is a traditional and more reasonable solution. Thus, extra batteries are applied as the ESS in this study. Figure 1 shows a typical household microgrid with PV power generation, ESS, and PEV.

1.3 Literature Review

When selecing the system structure, there are several considerations that need to be explored. One of them is to decide whether the charger of PEV should be connected to the DC side or the AC side. In literature, some studies addressed their research based on PEV charging themes with DC chargers. One [11] gave a review on PEV charging using PV power systems, which matched with the case defined in our study in many ways, except the scenario that is one with the main energy source being PV panels. Another study [12] demonstrated a similar configuration, which dedicated itself to the setup of charging stations for commercial buildings. Moreover, [13] used the same type of arrangement in the charging system of a parking garage designed for workplaces. To sum up, in real

applications, PEV charger connecting to DC side is suitable for the snenario of a parking lot with multiple PEV chargers.

In the meantime, for a scenario of household charging, an AC charger is often used. A typical PEV-grid charging system for individual household themes, as well as for most of the public PEV charging applications, is to implement AC PEV chargers [14]. It is capable of slow/normal and semi-fast/medium PEV charging, with a relatively low initial installation cost compared to DC fast charging stations [15]. To make the study more focused, a main scenario need to be decided. Because Level 2 charging, which requires a 240 V AC outlet, is typically described as the primary method for both private and public facilities [16], it is preferred that the PEV charger is connected to AC side.

Studies about microgrids include different models. Some studies focused on relatively large scale systems or power grids including three phase loads. Thus, it is reasonable to model the AC grid three-phased. Some studies focused more on power electronics, then the power electronic converters must be modeled. For this study, we are focusing on the energy management and its control strategy. Thus, from the control point of view, the energy flow of the system is the priority concern, and that is the reason the system is described as shown in Figure 1.

Different methods were explored for HEMS considering different microgrid architecture and optimization strategies. In [17], a rule-based control for HEMS with ESS was proposed. Since no optimization was involved, neither energy consumption nor cost minimization could be achieved. Although the minimization of load variances was discussed [1] [18], more literature was focused on energy cost optimization for a household microgrid. Different algorithms were applied to solve various mathematical optimization

problems, such as quadratic programming (QP) [1][18], stochastic dynamic programming (SDP) [19], and mixed-integer programming (MIP) [8][20][21][22]. In [20], mixed-integer linear programming (MILP) was used for HEMS optimization, with an additional feature of power factor maximization. In [21], the optimization was completed using a MILP solver and a heuristic technique separately. However, except [11], all aforementioned studies ignored the fact that the predicted values such as PV generation, load requirements might not equal to the actual value. Furthermore, the models of system dynamics might not be accurate enough. In [23], a modified stochastic predicted band was proposed to model uncertainties in the optimization problem. However, both [23] and [19] tried to model the uncertainty, but not compensate errors in the control.

There is also a growing trend for home appliances to pursue the concept of smart home or home automation. In other words, more control accesses are available to some of the load requirements. In [9], a concept of "soft load" was introduced. A soft load means that one load requirement has flexible scheduling and can be shifted from one period to another (e.g., washing machine and dryer). Although PEV's load requirement also falls into this category and can be regarded as a kind of soft loads, PEV loads might be unavailable if they are not at home. While flexible home loads are always available for charging. Thus, in this thesis, the term of the soft load is considered only for reschedulable household loads.

As a control method capable of handling constrained optimization problems, model predictive control (MPC) has been widely applied in various industrial applications, including power systems [8] [22] [24]. By integrating a receding horizon prediction, the measured values can be updated at each control step. As a result, the deviations of the actual energy production and load profile from forecasted values could be compensated

6

[24]. In [22], MPC was used in HEMS to compensate the uncertainty of predicted values. However, the focus was mainly on HEMS without ESS and PEVs. In [8], MPC was used in a HEMS with PEV, which assumed the PEV battery as the only ESS. Thus, the complexity of the scheduling problem was reduced because there was only one control variable. As discussed before, the PEV battery is not an optimal selection as an ESS.

1.4 Objectives

A HEMS using MPC for a practical and reasonable microgrid configuration, shown in Figure 1, is explored in this paper. The system has both DC and AC buses linked together using a bi-directional DC-AC converter. PV modules and battery packs are all connected to the DC bus with a DC-DC converter. AC bus is connected to both the grid and the loads, and the loads include both household loads and EV charging loads.

Moreover, with the trend of the smart home, users are given more control access to the home appliances. Thus we can also schedule some of the household load. The soft load is also considered and integrated into the MPC framework in this paper. Thus, there are multiple control variables, including the charging and discharging of the ESS, the charging of PEV as well as soft load scheduling. With the proposed MPC structure, it will be easy to compare different price plans, including consumer only or prosumer choices, and decide which plan gives the optimal result. In the simulation, different strategies of system operations based on different utility price plans are compared. To the authors' best knowledge, this is the first study that focuses on HEMS, with the presence of ESS, PEV, and electric soft loads using MPC for optimal scheduling in a household microgrid.

7

This thesis is mainly expanded from my submitted conference paper [25], the paper includes a large part of my work as a graduate student under the guidance of Prof. Yan Chen. Another part of my work relates to the development of the microgrid prototype, which is described in Chapter 4.

The remaining part of this thesis is organized as follows. In Chapter 2, modeling of systems in the household microgrid is introduced. In Chapter 3, the hardware prototype is introduced. Chapter 4 described the model predictive control theory. In Chapter 5, the problem formulation of HEMS and the MILP algorithm used to solve the MPC is discussed and investigated. Chapter 6 provides the simulation parameters and results, together with explanations and discussions. The conclusions are made in Chapter 7.

CHAPTER 2. OVERVIEW OF MODELS

The system, shown in Figure 1, consists of several components, whose model will be introduced part by part in this chapter. These model include equality and inequality relationships representing physical nature of these components. All the models of system components are combined together as constraints for the optimization problem. The objective function and the corresponding reformulations will be shown in the next chapter.

2.1 Notations

A prediction term represented in the form of $value(k|t)$ means the value predicted for step k at time t.

Symbol	Description
Power parameters/variables	
$P_{grid}(k|t)$	The power flow (in W) goes into/sell to the utility grid (< 0) or comes from/by from the utility grid (> 0).
$\tilde{P}_{gen}(k|t)$	Predicted value: the energy generated (in W) by PV panels.
$\tilde{P}_{load}(k|t)$	Predicted value: the un-schedulable load requirement (in W) for HEMS.
$\tilde{P}_{evconj}(k|t)$	Predicted value: the consumed energy (in W) of j_{th} PEV when driving.
$p_{evj}(k|t)$	Charging power (in W) of the PEV.
$p_{ess}(k|t)$	Charging/discharging power (in W) of the ESS.
$p_{sload}(k|t)$	Power for soft load requirements.
P_{grid_min}	Lower bound of power flow $P_{grid}(k|t)$.
P_{grid_max}	Upper bound of power flow $P_{grid}(k|t)$.
J_{max}	Upper bound of total electricity consumption in the household.

J_{sload}	Upper bound of total soft load consumption in the household, an integer multiple of p_{sload}.
P_{ev_char}	Upper bound for charging power of PEV (> 0).
P_{ess_char}	Upper bound for charging power of ESS (> 0).
P_{ess_dis}	Upper bound for discharging power of ESS (< 0).
P_{sload_dis}	Fixed number of power rating for soft load requirements.

Battery parameters/variables	
$b_{evj}(k)$	Battery charge (in Wh) of the j_{th} PEV at time k.
$b_{ess}(k)$	Battery charge (in Wh) of the ESS at time k
B_{evj_init}	Initial value of b_{evj}.
B_{evj_min}	Lower bound of b_{evj}.
B_{evj_max}	Upper bound of b_{evj}.
B_{ess_init}	Initial value of b_{ess}.
B_{ess_min}	Lower bound of b_{ess}.
B_{ess_max}	Upper bound of b_{ess}.

Indicating variables	
η_{ev_char}	PEV charging coefficient.
η_{ess_char}	ESS charging coefficient.
η_{ess_dis}	ESS discharging coefficient.
$\tilde{\gamma}_j(k\|j)$	Predicted value: whether j_{th} PEV is connected to HEMS ($= 0$) or not ($= 1$).
$price^+(t)$	Electricity purchase rate (> 0).
$price^-(t)$	Electricity sell rate (> 0).
M	Total number of PEVs

N	Horizon length of MPC
T	Total iteration steps

2.2 Prediction Models

System dynamics in the formulation of MPC have characteristics of evolving in a receding horizon. The finite horizon of future states with a fixed length is continually shifted for optimization from one-time step to the next. Thus, the predicted values, together with pricing variables, have to be formatted to fit into the receding horizon control.

The predicted values mainly consist of three parts: PV generation $\tilde{P}_{gen}(k|t)$, home load forecasting $\tilde{P}_{load}(k|t)$ and PEV states forecasting $\tilde{P}_{evconj}(k|t)$, $\tilde{\gamma}_j(k|t)$. These are all day-ahead predictions and are updated in every iteration step along with the receding horizon of MPC. All predictions could be obtained through probability distribution models using historical data [26].

For PV generation, different forecasting method can be applied. However, in cases where historical data can be accessed, a probabilistic model can be easily built using those statistical data via methods like Markov model [9] or autoregressive integrated moving average models (ARIMA) [27]. Household loads represent load requirement (except PEV charging requirement) in the home application, which can be described as schedulable and un-schedulable loads. The former, also called soft loads, is a type of load requirements that have flexible scheduling and can be shifted from one period to another (e.g., washing machine and dryer). In this study, the soft load is regarded as a control variable. The un-schedulable load could be predicted by an autoregressive model [8]. The leaving and arriving time of PEV could also be predicted using a semi-Markov model [8]. Moreover,

11

the predicted travel length and consumed power of PEV could also be predicted. To increase the credibility of the predicted values, the accuracy of the prediction can be increased by using improved models, larger historical data sets, or giving the user access to determine their next day usage *in prior*.

2.3 Power Balancing Models

The balance of the power in the household microgrid is represented from (1) to (4):

$$P_{grid}(k|t) = P_{load}(k|t) + P_{gen}(k|t) + \sum_{j=1}^{M} p_{evj}(k|t) \tag{1}$$
$$+ p_{ess}(k|t) + p_{sload}(k|t),$$

$$P_{grid\_min} \leq P_{grid}(k|t) \leq P_{grid\_max}, \tag{2}$$

$$\sum_{k=t}^{t+T-1} P_{grid}(k|t)\Delta t \leq J_{max}, \tag{3}$$

$$\sum_{k=t}^{t+(J_{sload}/P_{sload\_dis})-1} P_{sload}(k|t)\Delta t = J_{sload}. \tag{4}$$

Equation (1) represents that the power flow in/out of the utility grid equals to the sum of consumed fixed load power, generated power, PEV charging power, ESS charging/discharging power and soft load power consumption. The power flow in/out of the utility grid is constrained in (2). The total power usage of the household microgrid in a day is limited in (3). The constraint for the soft loads is described in (4). The soft load considered in this paper follows the definition of soft load Type B [9], in which the requirement has to be satisfied before the end of the simulation (usually a 24-hour period) and cannot be stopped once it is started until the requirements are fulfilled. The relationship between the power variables and coefficients are referred in Figure 1.

2.4 PEV and ESS Models

The model of PEV is described from (5) to (9).

$$b_{evj}(k+1|t) = b_{evj}(k|t) + \left[1 - \tilde{\gamma}_j(k|j)\right]\eta_{ev\_char}p_{evj}(k|t)\Delta t \tag{5}$$

$$- \tilde{\gamma}_j(k|j)\tilde{P}_{evconj}(k|t)\Delta t \,,$$

$$0 \le P_{evj}(k|t) \le P_{ev\_char} \,, \tag{6}$$

$$B_{evj\_min} \le b_{evj}(k) \le B_{evj\_max} \,, \tag{7}$$

$$P_{evj}(k|t)\tilde{\gamma}_j(k|j) = 0 \,, \tag{8}$$

$$b_{evj}(T) = B_{evj_{init}} \,. \tag{9}$$

Equation (5) stands for the state of charge (SOC) dynamics of PEV battery, while $\left[1 - \tilde{\gamma}_j(k|t)\right]\eta_{ev\_char}p_{evj}(k|t)\Delta t$ represents the change of SOC when connected to the household microgrid. $\tilde{\gamma}_j(k|t)\tilde{P}_{evconj}(k|t)\Delta t$ represents the change of SOC when the PEV is disconnected to the household microgrid. Although different factors can affect the battery's SOC and bring some randomness, such as route choices and traffic situations, only vehicle driving distance is considered in this paper for simplicity. The charging power and SOC are limited in (6) and (7), respectively. The condition that p_{evj} has an output only when PEV is connected to the HEMS is represented in (8). At the end of the simulation, the SOC of PEV is determined to be kept the same as the initial value in (9), which guarantees the usage of next day.

The model of ESS in the household microgrid, which is an industrial battery pack, is shown from (10) to (14).

$$b_{ess}(k+1|t) = b_{ess}(k|t) + E(k)p_{ess}(k|t)\Delta t, \tag{10}$$

$$\text{where } E(k) = \begin{cases} \eta_{ess\_char} & \text{if } p_{ess}(k|j) \geq 0 \\ \eta_{ess\_dis} & \text{if } p_{ess}(k|j) < 0 \end{cases},$$

$$P_{ess\_dis} \leq P_{ess}(k|t) \leq P_{ess\_char}, \tag{11}$$

$$B_{ess\_min} \leq b_{ess}(k|t) \leq B_{ess\_max}, \tag{12}$$

$$P_{load}(k|t) + P_{sload}(k|t) + P_{ess}(k|t) \geq 0, \tag{13}$$

$$b_{ess}(T) = B_{ess\_init}. \tag{14}$$

Equation (10) stands for the dynamic of ESS battery SOC. The charging power and the battery SOC are limited in (11) and (12), respectively. (13) prevents the ESS from selling the power to the utility grid. At the end of the simulation, the SOC of ESS has to be kept the same as the initial value, as described in (14).

CHAPTER 3. A PROTOTYPE OF MICROGRID

3.1 Development of Microgrid Prototype

In the study of the microgrid, the importance of experiments other than software simulation has been noticed. With a developed prototype, the proposed control theories and algorithms can be verified. In this part, a prototype microgrid, which intends to physically represent the target microgrid that is studied, has been developed.

To accurately represent the household microgrid, considering the specific characteristics, a downscaled microgrid prototype is preferred. Specific requirements of the prototype are listed:

1. The prototype needs to be a downscaled representation of the real microgrid, the voltage (RMS value) of the AC bus needs to be lower than 110V.

2. From the system design shown in Figure 1, a central controller is needed. The inverter and all the DC-DC converters need to be controlled by the central controller.

3. Since the system is designed to be grid-connected, a transformer is needed for connecting the low-voltage prototype AC bus to the 110V utility grid.

4. Photovoltaic panel modules and battery storage as ESS are needed.

5. A variable representation of home load and PEV loads need to be present.
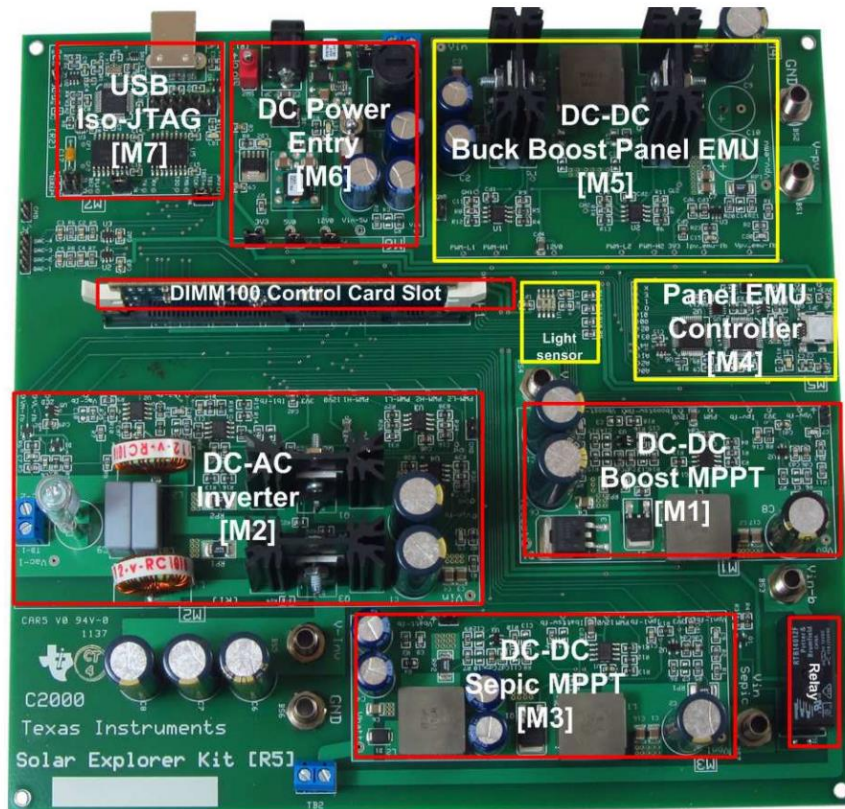
Figure 2. Macro Block on Solar Explorer Kit.

Based on the requirements, a development board named Solar Explorer Kit (Part Number: TMDSSOLARPEXPKIT), produced by Texas Instruments [28] was selected as the main component of the microgrid hardware prototype. It integrates multiple parts that fit the microgrid system design. This board uses TMS320F28035 ControlCARD microcontroller [29] as the central controller. It has a built-in PV emulator and an ambient light sensor that mimics the PV generation so that the experiment can be completed indoor without the physical PV modules. The board has a DC-DC boost converter for Maximum Power Point Tracking (MPPT) technique. Furthermore, a DC-DC SEPIC converter for battery charging is present. The development board also has a single-phase DC-AC inverter that can be used for the grid-connected mode. The macro blocks of the Solar Explorer Kit

16

is shown in Figure 2. In addition to all the converters and the inverter, the board has interfaces for connection of the external components, such as a real PV panel.

Based on the development board, other parts for the prototype microgrid are also integrated. Other than the built-in PV emulator, a 50W PV Panel module is used for a physical representation of PV generation. Moreover, an external battery pack is added to represent the ESS. Since the prototype is a scaled-down system, it cannot connect to the utility grid directly, thus a variable transformer is used for utility grid connection. The transformer is connected to the utility grid, and the other side of the transformer is connected to the AC side of the built-in inverter on the development board. To measure the currents, two AC current sensors are utilized, and an Arduino Uno microcontroller [30] is used to monitor the sensor outputs. The prototype is shown in Figure 3.

Figure 3. Prototype of the microgrid.

3.2 Demonstrations of two experiments

In this section, two experiments are demonstrated using the microgrid prototype. The first experiment represents a scenario where the HEMS is grid-connected with PV

generation, and no battery is present. The second experiment represents a scenario where the HEMS with PV generation is in island mode. The battery is charged in the daytime, and the load requirements representing street lamps are satisfied at night using energy from the battery. The software for control programming is Code Composer Studio provided by Texas Instruments.

The first demonstration is a grid-connected inverter system with photovoltaic modules. The experiment procedure is introduced in the manual [31] provided by Texas Instruments. The system diagram is shown in Figure 4. The system is connected to the utility grid, while PV is presented as a renewable energy source.

A DC-DC converter is connected to the PV output for MPPT. With a given fixed environmental condition, the PV modules only give the maximum output under a specific voltage/current. The control goal for the DC-DC converter is to make sure that the PV side has a voltage that ensures the PV's maximum power output. The algorithm to find the optimal voltage/current is called MPPT.

A DC-AC inverter is connected to the DC-DC to link the AC bus and DC bus. A variable AC-AC transformer is connected to the 110V utility grid.
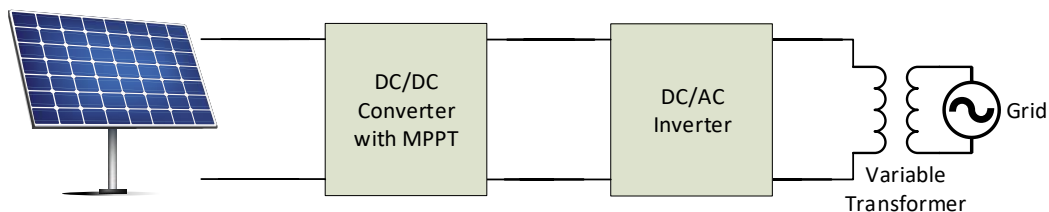

Figure 4. System Diagram of Grid-Connected Mode.

The experimental results of the first demonstration is shown in Figure 5. In the experiment, a 12 ohms resistor is used as the AC load and the voltage of DC bus is regulated

18

to 30 Volts. From the "experiment" plots in Figure 5, we can see that around 40 seconds, the output power of PV reaches its maximum, and the voltage of DC bus reaches its desired value. The reason that the MPPT function starts around 40 seconds is that during this time, the voltage of AC is gradually increasing, and finally reaches 12 RMS volts. The logic of the control is when the voltage of AC reaches 12 RMS Volts, the control system considers the AC voltage normal. Then the system checks if the voltage of PV panel is greater than 3V. If yes, the MPPT algorithm kicks in. The "simulationavg" plots are the flat lines in Figure 5, and it's from the simulation of the prototype system using MATLAB/Simulink, where average models of power electronics parts are being used. For average models that are used in various calculations and simulations, the transient responses are omitted and the models only focu on the steady state response. The "simulation" plots are the dashed line in Figure 5, and it's from the simulation of the prototype system using PLECS, a professional software for power electronics' design and simulation. In these plots, the system dynamics are considered. However, both "simulationavg" and "simulation" plots started simulation with the 12V AC voltage and MPPT initiated, whereas in real experiment, to protect the equipment, the AC voltage was being gradually increased. That's the reason why the "experiment" plots are displaying patterns different from the other two sets of plots.
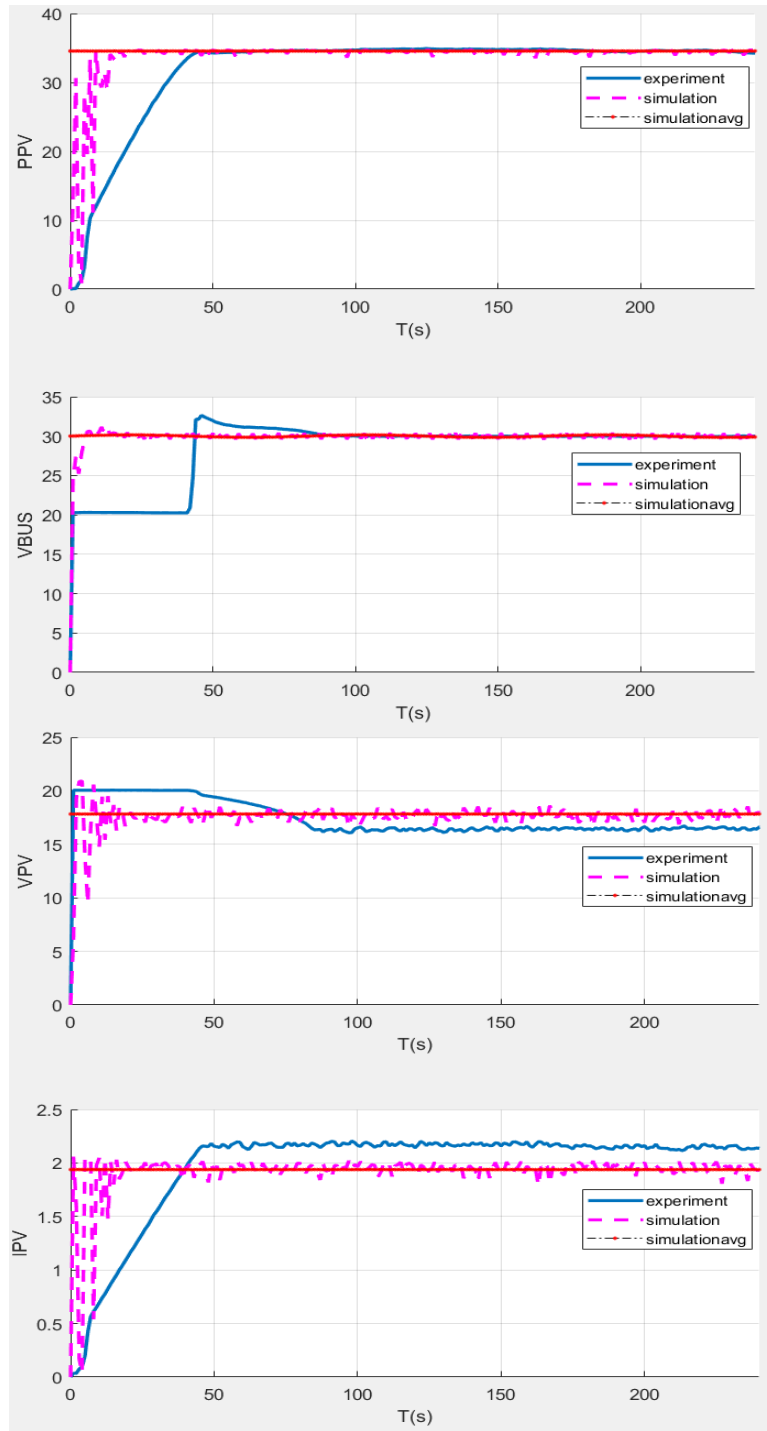
Figure 5. System Diagram of Grid-Connected Mode.
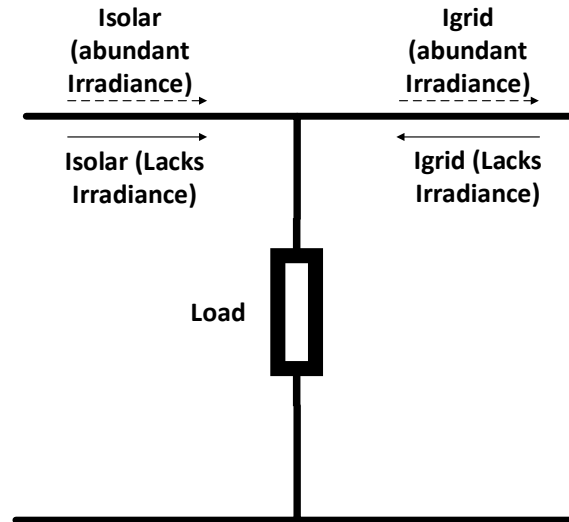
Figure 6. Relationship of Igrid and Isolar
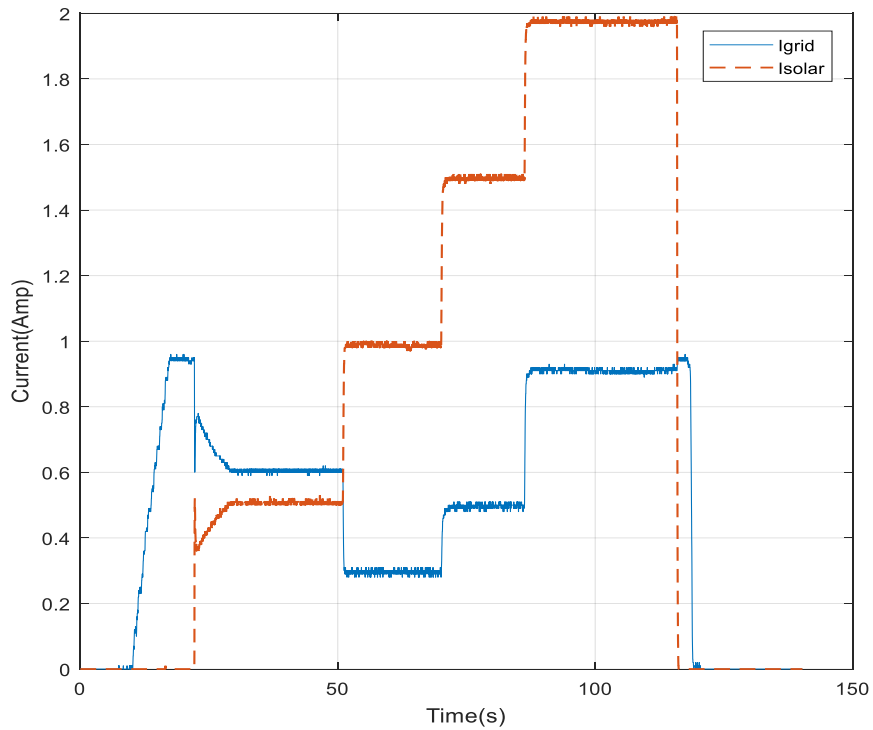
Figure 7. Energy Flow Diagram

In Figure 7, the energy flow diagram of the first experiment under various irradiance
levels is shown. The energy flow pattern varies along with the changes in irradiance levels.
The irradiance level is a variable that can be adjusted in the PV emulator of the
development board. The dash line *Isolar* represents the RMS value of AC current from

the PV side, and the solid line $Igrid$ represents the RMS value of AC current from the utility grid side. Both the currents are measured through current sensors. The load representing the system AC load is placed as shown in Figure 6. Since the current sensors only give a RMS values, the direction of the currents is mainly analyzed. Before 70th second, the irradiance level is not abundant, which means both the $Isolar$ and $Igrid$ have to satisfy the load requirement together. After 70th second, the irradiance level is abundant for producing enough power to satisfy the load requirement, and the irradiance level grows afterwards. Energy flows with respect to different irradiance levels are shown in Figure 6.
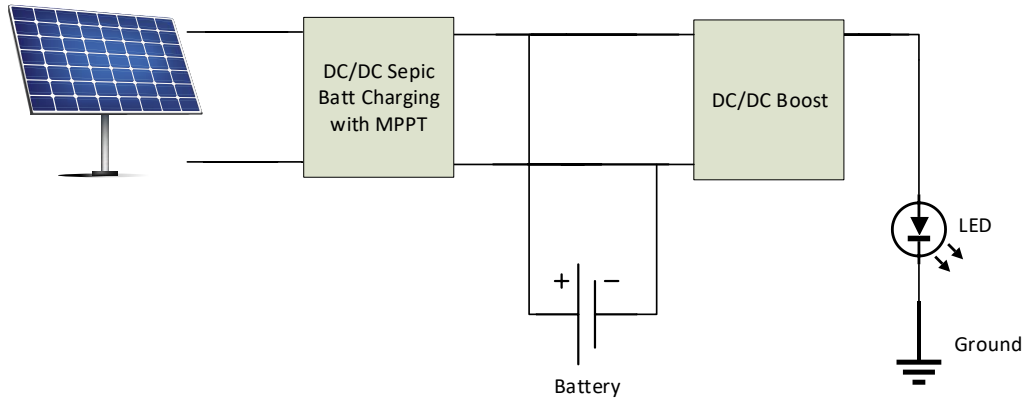

Figure 8. Diagram of PV Street Lighting System.

The second demonstration is a PV street lighting system. The experiment process is introduced in the manual provided by Texas Instruments [32]. The system diagram is shown in Figure 8. In this experiment, the system operates in island mode. The system utilizes PV as a renewable energy source, while the external battery is connected to the system storing the energy generated by PV in the daytime. At nighttime where the lighting system should be working, the external battery releases the energy to power the street light. The DC-DC converter used for MPPT in Figure 4 is now used as a DC-DC boost converter, while a DC-DC SEPIC converter is used for MPPT and battery charging purpose.

22

Since the characteristic of the street-light system does not quite fit the target system in this study, with a comprehensive understanding of the control logic, this demonstration has not been put into practice.

3.3 Software for Microgrid Prototype

The C2000 Controller utilizes two software applications. The first software is controlSUITE [33], which includes demo programs along with supporting documents for all C2000 microcontrollers, the other software is Code Composer Studio (CCS) Integrated Development Environment (IDE) [34] developed by Texas Instruments for code programming and compiling, shown in

Figure 9. The languages used for the controller are C++ and Assembly language. For Arduino microcontroller, Arduino IDE is utilized to get the current sensor read value.
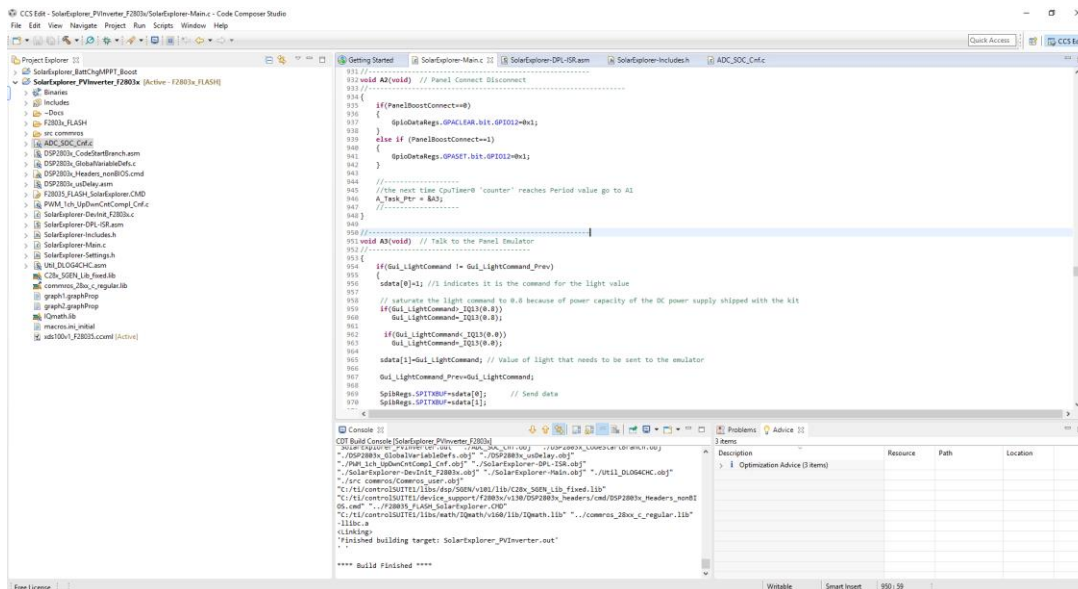
Figure 9. Interface of Code Composer Studio.

23

3.4 Future development for Microgrid prototype

With the aforementioned two demonstrations: grid-tied inverter system and PV battery lighting system, the future work will be to integrate these two system configurations into one architecture, which means the system is connected to the utility grid while has the ability to charge the battery, shown in Figure 10. By doing this, a physical representation of the grid-connected HEMS with the presence of PV and ESS will be constructed.
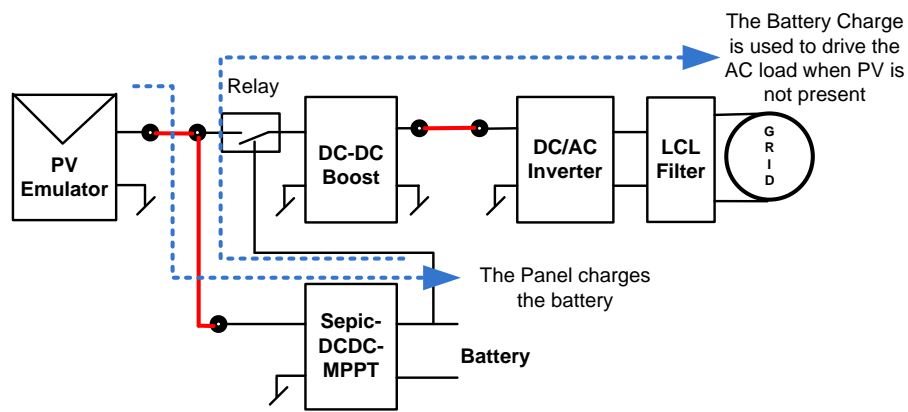
Figure 10. Diagram of Integrated System.

CHAPTER 4. MODEL PREDICTIVE CONTROL

As a widely implemented control strategy, model predictive control (MPC) is briefly introduced in this chapter. A detailed description of MPC can be found in reference [35].

4.1 Introduction of control systems

The basic concept of control systems is introduced as follows. The block diagram of a closed loop control system can be shown in Figure 11.

The input variables represent the control inputs, and the measured output variables are
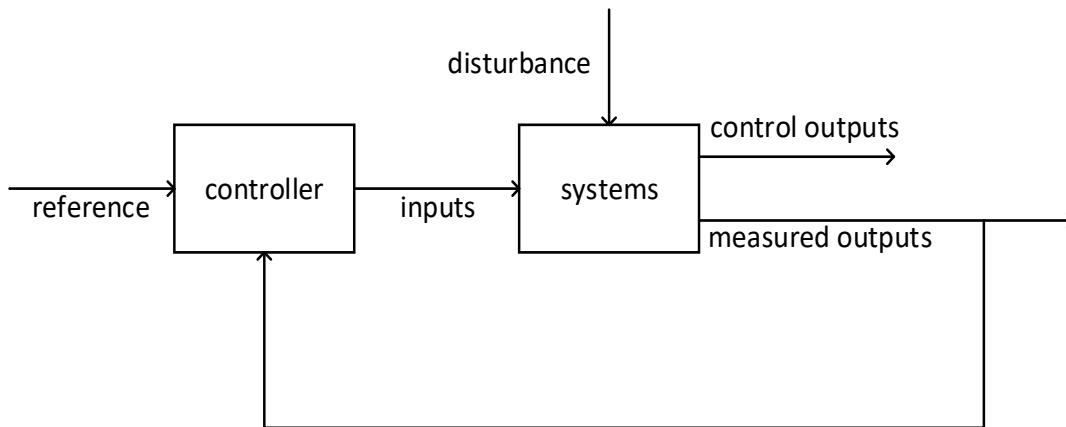
Figure 11. Diagram of Control System

used for feedback control. The system model can be either linear or nonlinear. Typically, the models for dynamic systems cannot adequately represent the real physical systems due to model uncertainties and/or disturbances, which are undesirable. The control objectives are defined in a way that the controlled outputs will track the given reference signals, and the tracking performance along with the closed-loop stability is guaranteed.

4.2 Introduction of MPC

MPC can be used as a control method for dynamic optimization problems. In MPC, both the control efforts and the responses of system states in the future are predicted. MPC has been widely implemented in various industrial applications. The basic idea of MPC is to predict future control inputs and state responses within regulated time intervals. MPC has the ability to control multiple variables, which makes it applicable in many industrial scenarios. Furthermore, by implementing various types of solvers for optimization problems, MPC is capable of dealing with different constraints representing the physical problems and limitations, which are considered in the problem-solving process of optimization. Given a long enough samplig time in MPC, the problem could be solved in real-time, and the receding horizon mechanism ensures the control performance. Thus, in some scenarios and textbooks, MPC is also called Receding Horizon Control (RHC).

The history of MPC can be traced back to early 1960's, where MPC was developed and a linear quadratic regulator (LQR) was designed. Then, through different improvements, many advanced MPC methods were proposed, such as Model Predictive Heuristic Control (MPHC), Dynamic Matrix Control (DMC) and Quadratic Dynamic Matrix Control (QDMC). Modern MPC can be regarded as the 4th generation of MPC which was developed in late 1995. A more detailed description of the MPC history is shown in [36].

4.3 Concept of MPC

Different from traditional control methods, MPC has a characteristic of finite horizon control. In traditional optimization methods, control system tends to run for a period

sufficiently long enough to guarantee that the optimized results are accurate. For this process, infinite horizon control is required. Different from the infinite horizon control, the basic concept of MPC is described as follows.

MPC obtains optimal control results at the current time, with a predefined time horizon. For example, if the current time is time k, then the calculated optimal control results with the fixed horizon are in time $[k, k + N]$, N is called the prediction horizon. After obtaining the optimization results, only the first control effort at time k will be used as a current control input. This procedure will repeat at the next time step $k + 1$. Namely, the calculated optimal controls are in time $[k + 1, k + N + 1]$ and the first control result for this step is at time $k + 1$. Thus, the time period of the optimal control results is moved from time $[k, k + N]$ to time $[k + 1, k + N + 1]$. The horizon length remains the same while the horizon itself moves, or "recedes" for the length of one time step. In this way, the term "receding horizon" is explained. MPC has been widely used in the process industry area as an alternative algorithm compared with the conventional PID control, which is short for proportional integrate derivative control. Different from PID control, which does not need a model (but an error) of a system, MPC is a model-based control and a system model is always required.

4.4 Advantages of MPC

MPC has drawn substantial interests in both academia and industry field, and it is proven to be a successful control theory that can be applied in various process controls. Several advantages of MPC [35] are listed below.

- MPC has the capability to be applied to a broad class of systems. Since MPC optimizes the problem over the finite horizon instead of infinite, systems such as nonlinear systems or time-delayed systems are all compatible with MPC.

- MPC provides a reliable approach for closed-loop control. Typically, numerical optimization methods are applied as open-loop controls. However, due to the repeated, feedback characteristics of MPC where only the first control is implemented, the closed-loop control can be guaranteed.

- The capability of handling constraints. For problems with constraints, MPC can be implemented with various types of mathematical programming methods, such as linear and nonlinear programming. These programming methods are able to handle the constraints of the optimization problems.

- MPC gives a good tracking performance. Theoretically, infinite horizon control that includes all future reference signals can provide the ideal tracking. However, in real application, the infinite horizon is hard to achieve. On the other hand, some control methods use "no horizon". In industry, PID is widely used, which is a control method that only takes the current reference, even with future reference available. Finite horizon provides a practical way of balancing the infinite horizon control and "current-reference-only" control. With an appropriate finite horizon length determined, MPC provides acceptable tracking performance.

- MPC can deal with parameter changes in the system. In the infinite horizon control, if the system parameter changes, the control cannot be adjusted because it will only be calculated once at the beginning. However, for MPC, it is

repeatedly calculated, and thus it can be easily adjusted for any parameter changes. In other words, MPC can be used for time-varying systems.

Due to the advantages stated above, MPC is widely used in industrial applications, where there are constraints for inputs and system states. Generally, some conventional control methods can meet the control requirements under constraints. However, they tend to be not the optimal operation, but behaves conservatively to guarantee the constraint requirements. MPC provides a more optimized solution. Morever, with the development of advanced computational power, real-time implementation of MPC for some small sampling time systems becomes more and more achievable.

4.5 Predictive control strategy

The system dynamic model is shown as:

$$x(k + 1) = Ax(k) + Bu(k) \,,$$

where $x(k)$ and $u(k)$ are model states and control inputs, respectively, and they are all vectors containing states of future N steps. The inputs and model states has the form of following:

$$x(k) = \begin{bmatrix} x(k + 1|k) \\ x(k + 2|k) \\ \vdots \\ x(k + N|k) \end{bmatrix}, \qquad u(k) = \begin{bmatrix} u(k|k) \\ u(k + 1|k) \\ \vdots \\ u(k + N - 1|k) \end{bmatrix}.$$

Given initial state $x(k|k)$ and given $u(k)$, the future states can be evolved as,

$x(k + 1|k) = Ax(k|k) + Bu(k|k)$, in gerenal,

$x(k + i + 1|k) = Ax(k + i|k) + Bu(k + i|k), \ i = 0,1 \dots$
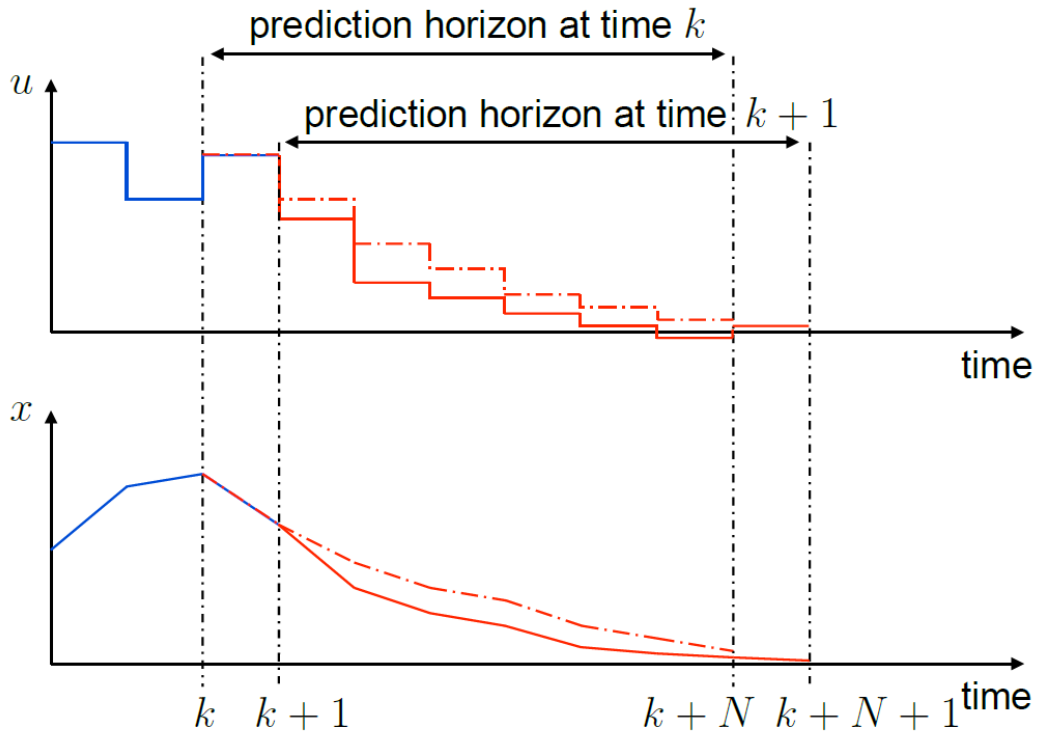
Figure 12. The receding horizon strategy from [35].

The receding horizon strategy means that the length of the horizon N remains the same within each control step. In the optimization problem with MPC, if the current time is k, at this time, the optimized inputs $u(k|k)$ to $u(k + N - 1|k)$ are calculated, and the control input of current time k is determined by the first optimized result $u(k|k)$. Then, it goes on to the time $k + 1$. At this time, the optimized inputs $u(k + 1|k + 1)$ to $u(k + N|k + 1)$ are calculated, and the control input of current time $k + 1$ is determined by the first optimized result $u(k + 1|k + 1)$. This control strategy goes on until the iteration stops. Since the fixed horizon is moving with the control time step, this charateristic is known as receding horizon strategy.

Figure 12 shows clearly that the horizon length remains the same with the horizon itself receding along with the time proceeds, and for each control step, the first optimized control input is applied.

There is no guarantee that the receding horizon mechanism of MPC can achieve an optimal solution. However, by evaluating MPC with infinite horizon prediction, this concern is addressed. The cost function for infinite horizon control could be defined as below:

$$J(k) = \sum_{i=0}^{\infty} \left(\left|\left|x(k+i|k)\right|\right|_Q^2 + \left|\left|u(k+i|k)\right|\right|_R^2 \right).$$

To make sure that in MPC, the cost minimization problem can be represented using finite variables, a transformation called dual-mode prediction is shown as:

$$u(k+i|k) = \begin{cases} \text{optimization variables} & i = 0,1,\dots,N-1 \quad \text{(mode 1)} \\ Kx(k+i|k) & i = N, N+1, \dots \quad \text{(mode 2)} \end{cases},$$

here N is the length of the prediction horizon. Mode 1 represents the variables in finite horizon and mode 2 defines the remaining infinite variables. With dual modes, $J(k)$ can be represented as:

$$J(k) = \sum_{i=0}^{N-1} \left(\left|\left|x(k+i|k)\right|\right|_Q^2 + \left|\left|u(k+i|k)\right|\right|_R^2 \right) + \left|\left|x(k+N|k)\right|\right|_{\bar{Q}}^2.$$

By choosing a proper terminal weighting matrix $\bar{Q}$, the cost under infinite horizon can be accounted in $J(k)$ under assumptions in mode 2. By rewritting to this form, only finite optimization variables are needed for infinite horizon evaluation by choosing proper $\bar{Q}$.

In this study, we will not consider the terminal weighting term $\left|\left|x(k+N|k)\right|\right|_{\bar{Q}}^2$, because for the problem that is discussed in this thesis, the prediction horizon is defined

for a fixed time. The infinite horizon prediction cannot be achieved due to the characteristics of the microgrid system, where only limited information about the future will be known for users. The information includes variables, such as future load requirements and the vehicle status, which in reality, are predicted from history data. Future data with infinite horizon cannot be accurately predicted from the history, and thus make the effort of achieving an optimal solution with infinite prediction horizon impossible and unnessasary. Also, in this thesis, a linear prediction plant model will be used, and the cost $J(k)$ can be represented as a quadratic function of the inputs only, without the presence of system states, which will be illustrated in the next chapter.

CHAPTER 5. PROBLEM FORMULATION

In this chapter, Mixed-integer-linear-programming (MILP) structure is introduced. Due to the nonlinear nature of the desired problem, it can not be directly formulated into MILP, the method reformulating the problem to fit the MILP is described.

5.1 MILP Structure

Mixed-integer-linear-programming is a mathematical optimization algorithm that allows some part of the inputs to be integers. A MILP algorithm is formulated as follows:

$$\min_x c^T x \text{ subject to} \begin{cases} x(\text{intcon}) \text{ are integers} \\ A \cdot x \leq b \\ Aeq \cdot x = beq \\ lb \leq x \leq ub \end{cases}, \qquad (15)$$

where c, x, intcon, lb, ub, b and beq are vectors, and A and Aeq are matrixes. For an optimization problem, $\min_x c^T x$ denotes the minimum value of $c^T x$, for the optimum value of variables chosen among their regions. Aside from the objective function, constrains are often involved representing limits of the control inputs or system states due to different characteristics of the specific problem that is being solved.

5.2 Problem Reformulation

The optimization goal of the HEMS is to minimize user's cost of electric power. The problem is formulated in an MPC configuration solved by MILP algorithm, which has the capability to handle the binary variables representing decision variables.

The objective function is written as (16):

$$\min J = \sum_{k=t}^{t+T-1} R(k)P_{grid}(k|t)\,\Delta t + \Delta D, \tag{16}$$

where $R(k) = \begin{cases} price^+(k) & \text{if } p_{grid}(k|t) \geq 0 \\ price^-(k) & \text{if } p_{grid}(k|t) < 0 \end{cases}$, and

$$\Delta D = \alpha_{\text{ess}} \sum_{k=t}^{t+T-1} D_{ess}(k|t) + \alpha_{\text{ev}} \sum_{k=t}^{t+T-1}\sum_{j=1}^{M} D_{evj}(k|t).$$

In (16), ΔD is a penalty term limiting the sudden change of both p_{ess} and p_{evj}. α_{ess} and α_{ev} are penalty weightings. D_{ess} and D_{evj} can be regarded as a control input with constraints shown from (17) to (20):

$$D_{ess}(k|t) \geq p_{ess}(k|t) - p_{ess}(k-1|t), \tag{17}$$

$$-D_{ess}(k|t) \leq p_{ess}(k|t) - p_{ess}(k-1|t), \tag{18}$$

$$D_{evj}(k|t) \geq p_{evj}(k|t) - p_{evj}(k-1|t), \tag{19}$$

$$-D_{evj}(k|t) \leq p_{evj}(k|t) - p_{evj}(k-1|t). \tag{20}$$

Equations (10) and (16) are not linear, because the value of $E(k)$ and $R(k)$ are determined by logic and thus cannot be directly implemented in MILP algorithm. As a result, some reformulation needs to be done.

The methodology to transfer the problem into MILP framework, by using the method in [37], is described below.

In many applications, the model of the system includes parts that need logic determination. For the specific problem that this paper is trying to solve, the model includes E and $R(k)$, the value of which depends on whether $p_{ess}(k|t)$ or $p_{grid}(k|t)$ is positive or negative, respectively. To address this characteristic, logical variable $\delta \in \{0,1\}$ is

introduced, the value of this binary integer variable represents the logical determination,

and can be implemented into MILP framework. Thus, we have:

$$\begin{cases} [\delta_E(k|t) = 1] \leftrightarrow [p_{ess}(k|t) \geq 0] \\ [\delta_E(k|t) = 0] \leftrightarrow [p_{ess}(k|t) < 0] \end{cases}, \tag{21}$$

$$\begin{cases} [\delta_R(k|t) = 1] \leftrightarrow [p_{grid}(k|t) \geq 0] \\ [\delta_R(k|t) = 0] \leftrightarrow [p_{grid}(k|t) < 0] \end{cases}. \tag{22}$$

Logical variables representing the logic determination on the value of variable $E(k)$

and variable $R(k)$: $\delta_E(k|t) \in \{0,1\}$, $\delta_R(k|t) \in \{0,1\}$, and the auxiliary variables

$\begin{cases} z_E(k|t) = \delta_E(k|t)p_{ess}(k|t) \\ z_R(k|t) = \delta_R(k|t)p_{grid}(k|t) \end{cases}$ are introduced. Thus, (10) is rewritten as equations from

(23) to (29):

$$b_{ess}(k+1|t) = b_{ess}(k|t) + [(\eta_{ess\_char} \tag{23}$$
$$- \eta_{ess\_dis})z_E(k|t) + \eta_{ess\_dis}p_{ess}(k|t)]\Delta t,$$

$$z_E(k|t) \leq \delta_E(k|t)P_{ess\_char}, \tag{24}$$

$$z_E(k|t) > \delta_E(k|t)P_{ess\_dis}, \tag{25}$$

$$z_E(k|t) \leq p_{ess}(k|t) - P_{ess\_dis}[1 - \delta_E(k|t)], \tag{26}$$

$$z_E(k|t) > p_{ess}(k|t) - P_{ess\_char}[1 - \delta_E(k|t)], \tag{27}$$

$$p_{ess}(k|t) \leq P_{ess\_char}[1 - \delta_E(k|t)], \tag{28}$$

$$p_{ess}(k|t) > (P_{ess\_dis} + \varepsilon)\delta_E(k|t) - \varepsilon, \tag{29}$$

where (23) is a linear representation of equation (10), $z_E(k|t) = \delta_E(k|t)p_{ess}(k|t)$ holds if

inequalities constraints from (24) to (27) are satisfied, whereas $\delta_E(k|t) =$

$\begin{cases} 1 & \text{if } p_{ess}(k|t) \geq 0 \\ 0 & \text{if } p_{ess}(k|t) < 0 \end{cases}$ holds if constraint (28) and (29) are satisfied.

Likewise, (16) can also be rewritten as (30) to (36):

$$\min J = \sum_{k=t}^{t+T-1} [\left(price^+(k) - price^-(k)\right)z_R \tag{30}$$

$$+ price^-(k)P_{grid}(k|t)]\Delta t + \Delta D \,,$$

$$z_R(k|t) \leq \delta_R(k|t)\text{P}_{\text{grid\_max}} \,, \tag{31}$$

$$z_R(k|t) > \delta_R(k|t)\text{P}_{\text{grid\_min}} \,, \tag{32}$$

$$z_R(k|t) \leq p_{grid}(k|t) - \text{P}_{\text{grid\_min}}[1 - \delta_R(k|t)] \,, \tag{33}$$

$$z_R(k|t) > p_{grid}(k|t) - \text{P}_{\text{grid\_max}}[1 - \delta_R(k|t)] \,, \tag{34}$$

$$p_{grid}(k|t) \leq \text{P}_{\text{grid\_max}}[1 - \delta_R(k|t)] \,, \tag{35}$$

$$p_{grid}(k|t) > (\text{P}_{\text{grid\_min}} + \varepsilon)\delta_R(k|t) - \varepsilon \,, \tag{36}$$

where (30) is a linear representation of equation (16), $z_R(k|t) = \delta_R(k|t)p_{grid}(k|t)$ holds if inequalities constraints from (31) to (34) are satisfied, whereas $\delta_R(k|t) =$

$\begin{cases} 1 & \text{if } p_{grid}(k|t) \geq 0 \\ 0 & \text{if } p_{grid}(k|t) < 0 \end{cases}$ holds if constraint (35) and (36) are satisfied.

Through transformation described above, the optimization problem can be constructed in the form of MILP algorithm. More specifically, the objective function for the MILP optimization is (30), the constraints are from (1) to (9), (11) to (14), and (17) to (36).

5.3 System Control Structure and Programming Realization

The system control structure, designed as a MPC controller, is described in Figure 13. The iteration starts with Prediction machine, where the value needed for constraints calculation is predicted (for prediction value) and processed (for price variables). Next, with the initial conditions defined, the constraints matrixes and vectors for MILP optimization (A, Aeq, b, beq, lb, ub) are calculated. With the objective function defined,

start

$t=1$

Prediction machine $t=t+1$

$price^{-}$
$price^{+}$ predictions

Constraints calculation

constriants

MILP for next N steps p_{sload} $t<T$ Y
p_{evj}
p_{ess} N

p_{ess}
p_{evj}

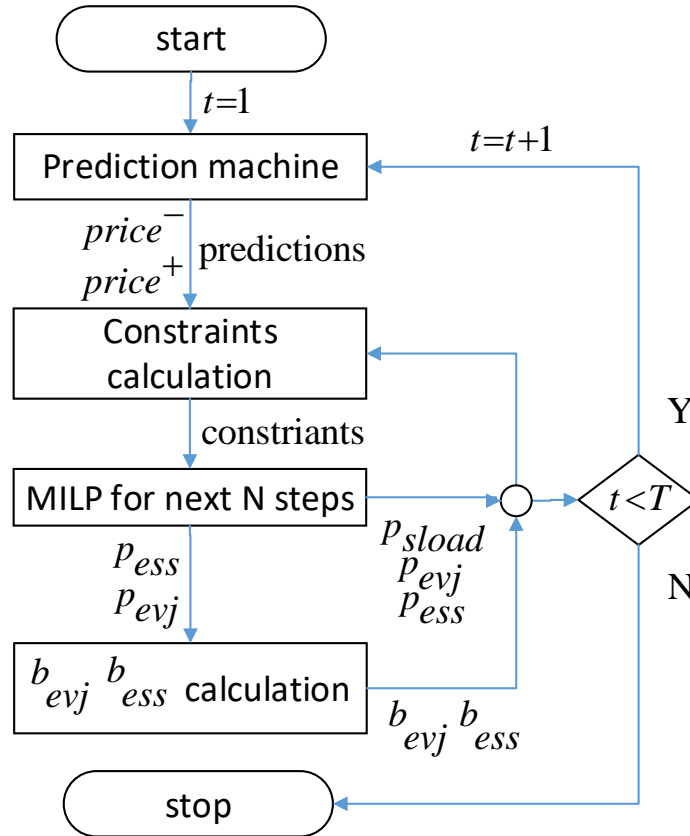b_{evj} b_{ess} **calculation** b_{evj} b_{ess}

stop

Figure 13. MPC control framework

MILP optimization will be done and optimized results of the next N steps for current iteration will be given. Using p_{ess} and p_{evj}, the SOC of PEV and ESS are b_{evj} and b_{ess} are calculated using dynamic battery models of PEV and ESS. For this step, in real applications, b_{evj} and b_{ess} can be measured and sent to the system, instead of esimation where errors are inevitable. Thus, the error between estimation using the battery model and real battery states can be compensated, which is one of the main strengths of MPC in this application. These values are then saved and will be sent to Constraints calculation in the next iteration. The next iteration starts over from pridiction machine, until the iteration number reaches the preset maximum value.

MPC has the characteristic to optimize the objective function in consideration of constraints and system dynamics, over a prediction horizon. Moreover, forecast profiles and measurements uncertainties can be updated in a receding horizon fashion, thus the forecast uncertainties can be handled by the receding horizon strategy [18], the error caused by system dynamic model can also be compensated.

Next, some detailed information about the programming realization will be discussed. From the description of the system modeling and control from previous parts of this article, the control input u within one time step can be described as a 11×1 vector $u = \left(P_{grid}\ \delta_E\ \delta_R\ z_E\ z_R\ P_{evj}\ P_{ess}\ D_{evj}\ D_{ess}\ Init_s\ On_s\right)^T$, $Init_s$ is a binary variable denoting the starting time of the soft load (when started, $Init_s$ equals to 1). The soft load requirements need to be fully satisfied once started, and no break in the middle is allowed. Thus, for one set of soft load, there is only one starting time, and correspondingly, $Init_s = 1$ only appears once in one simulation. On_s is also a binary variable indicating the time when the soft load requirement is being fulfilled (equals to 1). Thus, $P_{sload} = On_s \cdot P_{sload\_dis}$. From (15), the integer variables are defined as a representation of x(intcon). Therefore, for a 11×1 vector $u = \left(P_{grid}\ \delta_E\ \delta_R\ z_E\ z_R\ P_{evj}\ P_{ess}\ D_{evj}\ D_{ess}\ Init_s\ On_s\right)^T$ where the 2nd, 3rd, 10th and 11th element are binary variables, intcon $= [2,3,10,11]$. Furthermore, lb and ub are vectors used for storing the lower and upper limits of each variable. For MPC with a finite horizon N, the vector u needs to be applicable for all N control steps. As a result, in MPC for this system, the control input is a $N \cdot 11 \times 1$ vector, and intcon, lb and ub all need to be modified correspondingly with respect to N .

The prediction machine generates all predicted values. At time t, the predicted values from $(t|t)$ to $(t + N|t)$ are given. In this thesis, since the focus of the study is on the control algorithm, instead of the prediction methods, the prediction variables are pre-defined in the simulation. However, in real applications, the prediction methods and algorithms can be implemented into the prediction machine. Furthermore, due to the principle of MPC, the time-variant utility price is updated using the same form as predicted values, which is from $(t|t)$ to $(t + N|t)$. This structure can be used for implementation of dynamic pricing strategy [19].

After the predicted values are given, the constraint matrixes A, Aeq, b and beq in (15) can be determined. The constraints contain the information about the limitation of the physical system, as well as the system dynamics. There are two types of constrain representations, one type is equality constraints expressed by $Aeq \cdot x = beq$ while the other is inequality constraints expressed by $A \cdot x \le b$. Note that when constructing constraint matrixes, if the constraint does not contain system dynamics, the constrain is only related to variables in the current time step. For example, in (13): $P_{load}(k|t) + P_{sload}(k|t) + P_{ess}(k|t) \ge 0$, first it is transferred into $-P_{sload}(k|t) - P_{ess}(k|t) \le P_{load}(k|t)$, then the matrix A can be constructed. This constraint is related to control inputs $P_{sload}(k|t)$ and $P_{ess}(k|t)$. The psudo code for this contraint is shown as:

> For i=1:N
>   A(21*i-16,11*i-5) = -1
>   A(21*i-16,11*i-0) = -1
>   b(21*i-16) =$\tilde{P}_{load}(t + i - 1|t)$

,

where i stands for the time from present (i=1) to the horizon-time-step future (i=N). As stated before, the control input is a $N \cdot 11 \times 1$ vector, thus A(21*i-16,11*i-5) = -1 stands

for constraint number 21*i-16, for control input 11*i-5, which corresponds to $P_{ess}(t + i - 1|t)$ for every i within [1,N]. Similarly, A(21*i-16,11*i-0) = -1 stands for constraint number 21*i-16, for control input 11*i-0, which corresponds to $P_{sload}(t + i - 1|t)$ for every i within [1,N]. b(21*i-16) represents $P_{load}(t + i - 1|t)$.

Note that for constraints (4), (9), (14), certain requirements need to be fulfilled before the end of simulation. Since the horizon keeps receding, in the programming, the ending time for finishing the task needs to move forward along with the receding of the horizon to make sure that at the end of simulation, the requirements are met. For example, in (9): $b_{evj}(T) = B_{evj\_init}$, if the simulation time is 24 hours and horizon length is 24 hours, with an half-hour time step, so in total 48 time-step horizon. At the start of simulation, the constraint should be programmed as: $b_{evj}(48) = B_{evj\_init}$. Then, at the next time step of simulation, the constraint should be programmed as: $b_{evj}(47) = B_{evj\_init}$, and so on. At the last time step, it should be $b_{evj}(1) = B_{evj\_init}$.

Another type of constraint relates to system dynamics. For example, in (7): $B_{evj\_min} \leq b_{evj}(k) \leq B_{evj\_max}$, since $b_{evj}(k|t)$ is system dynamic shown in (5): $b_{evj}(k + 1|t) = b_{evj}(k|t) + [1 - \tilde{\gamma}_j(k|j)]\eta_{ev\_char}p_{evj}(k|t)\Delta t - \tilde{\gamma}_j(k|j)\tilde{P}_{evconj}(k|t)\Delta t$, which means that the current state relates to history states. Thus, when constructing constrains for system dynamics, historical states need to be considered. For (7), the constraints for $b_{evj}(k|t)$ are

first converted to $\begin{matrix} -b_{evj}(k|t) \leq -B_{evj\_min} \\ b_{evj}(k|t) \leq B_{evj\_max} \end{matrix}$, then based on (5), the psudo code is:

For i=1:N
    j = 1;
    while j <= i
        Consbev(j) = - $\tilde{\gamma}_j(t + j - 1|t) \cdot \tilde{P}_{evconj}(k|t)$
        Parb_pev(j) = (1- $\tilde{\gamma}_j(t + j - 1|t)) \cdot \Delta t \cdot \eta_{ev\_char}$

        A(21*i - 15, 12*j - 6) = -Parb_pev(j)
        b(21*i - 15) = b(21*i - 15) + Consbev(j);

        A(21*i - 14, 12*j - 6) = Parb_pev(j);
        b(21*i - 14) = b(21*i - 14) - Consbev(j);

        j = j+1;
    end
        b(21*i - 15) = b(21*i - 15) - Bevmin + bkev;
        b(21*i - 14) = b(21*i - 14) + Bevmax - bkev;

,

where i stands for the time from present (i=1) to the horizon-time-step future (i=N). Since all the N steps are calculated in one-time simulation, the dynamic state b_{evj} in each time step $(t + i - 1|t)$ $i = 1 \dots N$ is related to all previous states starting from the time step when i=1. A(21*i - 15, 12*j - 6) stands for constraint number 21*i-15, for control input 12*j-6, which corresponds to $P_{evj}(t + j - 1|t)$ for every j within [1,i]. Constraint number 21*i-15 represents $-b_{evj}(k|t) \leq -B_{evj\_min}$, while constraint number 21*i-14 represents $b_{evj}(k|t) \leq B_{evj\_max}$. It can be seen that along with the growth of i, the constraints 21*i – 15 and 21*i– 14 are involved with more and more elements because the larger i brings the more j candidates. These elements represent the relationship between current state and past states.

CHAPTER 6. SIMULATION RESULTS AND DISCUSSIONS

6.1 Simulation Setup

The simulation describes a typical household microgrid, where 6kW PV panel modules, 3kWh capacity ESS, and PEV battery are present. In the simulation, PV generation forecasting data for every half hour is from [17]. Hourly consumption data are obtained from [38] for a typical household in the US and then transferred into half-hour data by linear interpolation, which will be used as load prediction. The PV generation and load curve are shown in Figure 14. The PEV state estimation data is defined to match the designed scenes. Some parameters used are listed in Table I.
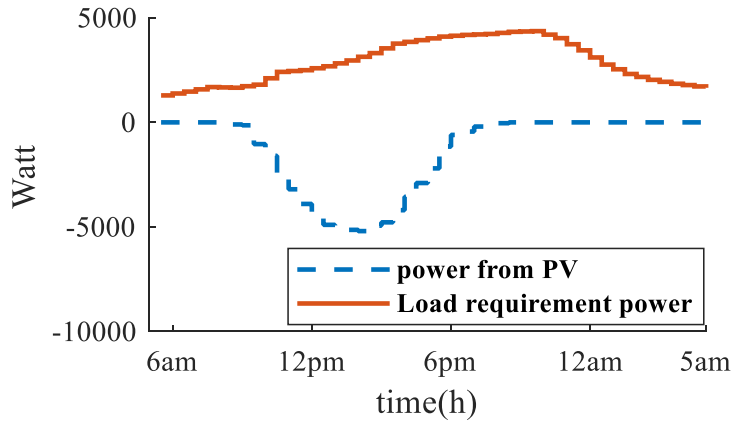

Figure 14. PV Generation & Load Requirement.

TABLE I

PARAMETER USED IN SIMULATION

Term	Value	Term	Value
B_{evj_init}	70000 Wh	B_{ess_init}	15000 Wh
B_{evj_max}	90000 Wh	B_{ess_max}	27000 Wh
B_{evj_min}	30000 Wh	B_{ess_min}	3000 Wh
η_{ev_char}	0.99	η_{ess_char}	0.99
$\alpha_{ess}, \alpha_{ev}$	0.01	η_{ess_dis}	1.01

42

The simulation duration is a 24-hour period, with a sampling time of 30 min. The starting/ending time for simulation is set to be at the 05:00 am of the day. Both states of charges in ESS and PEV are required to be equal to the initial values. Although the PEV can be theoretically charged at the last minute of the predicted usage time, the PEV should be charged at an earlier time considering that the prediction might not always be accurate. The vehicle was assumed to be a Tesla Model S P100D [39]. Based on the datasheet, for 45 mph speed with 90 degrees environment temperature, the vehicle can drive 455 miles. With calculation, the vehicle consumes power at 9900 Watt/hour. A commercial software CPLEX for Matlab Toolbox was used for solving the MILP optimization problem.

In the simulation, a typical workday scene is simulated. The scenario is chosen for a day between May and September, which matches the "summer peak time" set by South River Project Corp. (SRP). The PEV leaves home for work at 08:30 and arrives home at 16:30. From 8:30 to 9:00 and from 16:00 to 16:30, the user drives the PEV at 45 mph. For the rest of the time away from home, the vehicle remains idle. The soft load is chosen to be a 400-Watt washing machine. The requirement is 400 Wh and the duration is one hour, which needs two time periods to fulfill the requirement. The deadline for the soft load is set to be at the end of the iteration.

6.2 Different Cases

In this part, three cases will be studied. For all cases, the assumptions described above hold. The results are shown in Figure 15.
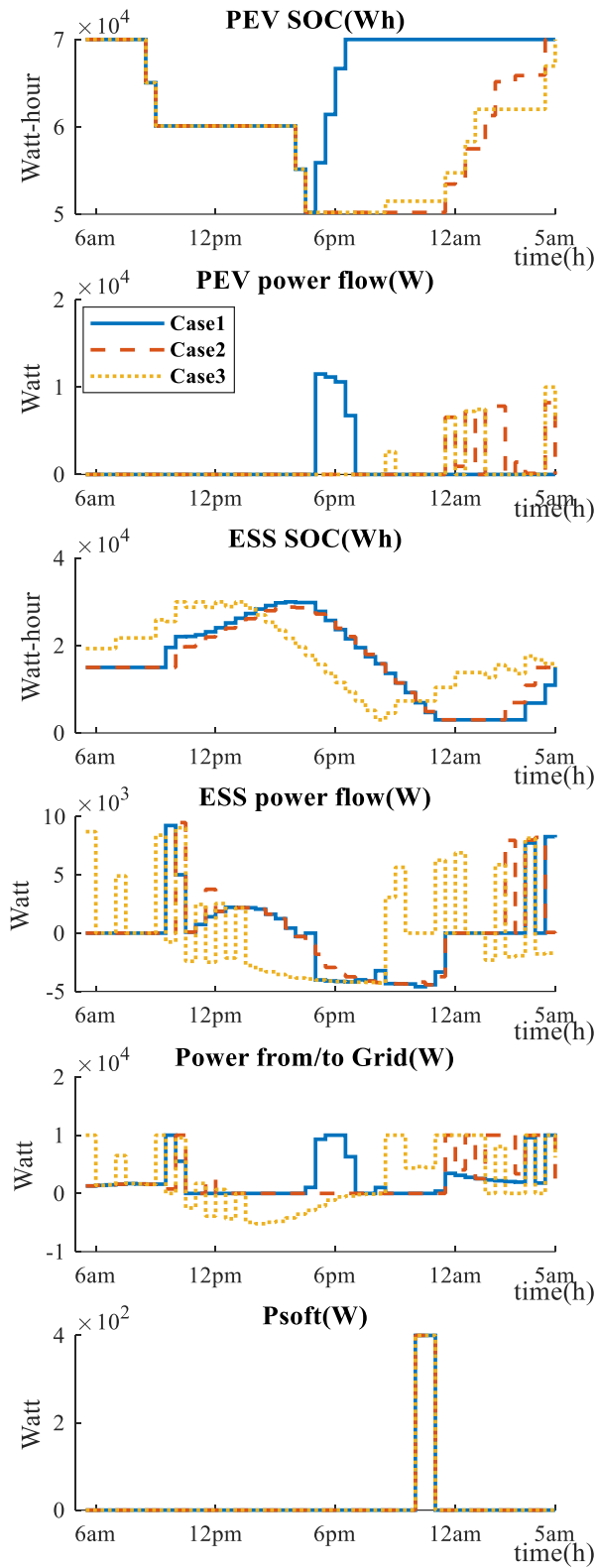
Figure 15. Power Flow & SOC for Case1, 2 and 3 respectively.

In Case I, no optimization is applied for PEV charging. In other words, PEV will start charging instantly once it is back home and being connected to the microgrid. However, the ESS is operating optimally. The price plan is based on SRP "Electric Vehicle Price Plan" [40]. In this case, selling the electricity to the utility grid is prohibited, which means the excess power flows either to ESS or directly to the load requirement. For soft load, all three cases have the same strategy, because the starting time is the lowest electricity price period. The final cost for Case I during one day is 13.79 dollars. Note that for soft loads, all three cases have the same scheduling patterns. The reason is that although the price plan varies, they all have the same kind of settings on the peak/valley periods. Thus, starting time of the soft load for three cases are always the starting time of the lowest electricity price period.

In Case II, the optimization is used in both PEV charging and ESS. The price plan is the same as Case I, and the function of selling electricity back to the utility grid is also not activated. In Figure 15, from "PEV SOC" and "PEV POWER FLOW (W)," it is shown that the charging time of PEV in Case II is chosen at a later time than in Case I, for less charging cost. The final cost for Case II during one day is 7.74 dollars, 43.9% lower than the instant charging strategy in Case I.

In Case III, SRP customer generation price plan [41] is used. This is the price plan option for SRP customers who consider selling their excess energy to the utility grid. The electricity price is the lowest among all price plans. However, the plan has a massive penalty for buying electricity at on-peak hours (1-8 p.m.). In Figure 15, from "power from/to grid," it is shown that the value of power goes below zero in the middle of the day, which matches the pattern of PV generation. The final cost for Case III during one day is

4.22 dollars, 69.4% lower than the instant charging strategy in Case I. Note that this cost reduction is based on the result that no energy is purchased from the utility grid during on-peak hours. Based on the price plan, the minimum penalty for every excess 1 kW purchased during on-peak hours is 9.59 dollars, and it can be even higher for more purchased energy. Adding the 1 kW penalty, the cost becomes 13.81 dollars, higher than Case I. Thus, for this price plan, amount of energy purchased during on-peak hours strongly affects uses' economic benefit. It can be readily seen that if there is not enough energy production capability, it is preferred to choose the "Electric Vehicle Price Plan" for more stable performance in achieving the optimal goal of cost reduction.

For comparisons, besides 6 kW PV generation, two other costs for 3 kW and 9 kW PV module are also shown in Table II and Figure 16. From the table, the costs among different generation capabilities display in a nearly-linear relationship. The user needs to balance the economic benefit, initial investment cost, and other aspects of maintenance cost and available rooftop area, to decide on how many generations capability a household needs. Note that for Case III, simulations with different generation capabilities pay no penalties. If the user prefers Case III, which is customer generation price plan, further consideration is needed when the penalty is within consideration for cases where extra energy has to be purchased from the utility grid during on-peak hours.

TABLE II
COST CALCULATION (DOLLAR)

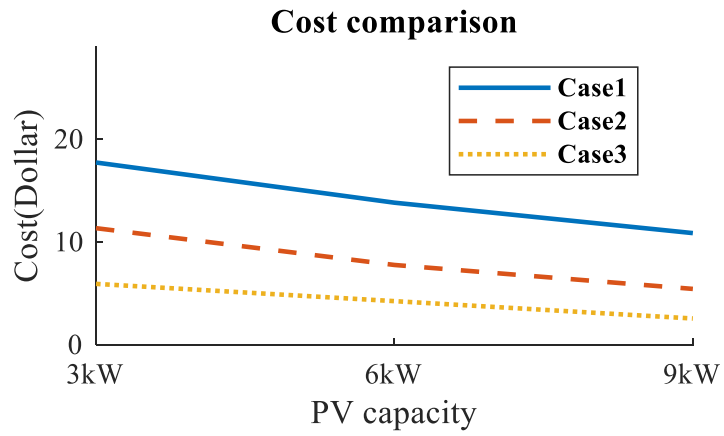|	3 kW	6 kW	9 kW
Case I	17.71	13.80	10.84
Case II	11.32	7.74	5.41
Case III	5.90	4.22	2.53

Figure 16. Cost for Case1 to 3 under different PV capacities.

CHAPTER 7. CONCLUSIONS

A household energy management strategy has been studied in this paper. An optimization method for PEV charging and strategy for HEMS with ESS and the soft load is considered, using the MPC method. Through comparisons of simulation results for different settings and price plans, the effectiveness of the optimization control is verified. Suggestions are given for user's economical benefits based on the simulation results. Further study can be made on 1) verification of the MPC capability for compensating estimation errors by conducting related experiments in a prototype microgrid; 2) methods to further smoothen the charging power.

REFERENCES

[1] Jian, L., Xue, H., Xu, G., Zhu, X., Zhao, D.,and Shao, Z.Y., "Regulated charging of plug-in hybrid electric vehicles for minimizing load variance in household smart microgrids," *IEEE Transactions on Industrial Electronics, vol. 60 (8),* pp. 3218-3226, 2013.

[2] Green II, R.C., Wang, L. and Alam, M., "The impact of plug-in hybrid electric vehicles on distribution networks: A review and outlook," *Renewable and Sustainable Energy Reviews, vol. 15 (1),* pp. 544-553, 2011.

[3] Wang, Q., Liu, X., Du, J. and Kong, F., "Smart Charging for Electric Vehicles: A Survey from the Algorithmic Perspective," *IEEE Communications Surveys and Tutorials, vol. 18 (2),* pp. 1500-1517, 2016.

[4] Bhatti, A.R., Salam, Z., Aziz, M.J.B.A., Yee, K.P. and Ashique, R.H., "Electric vehicles charging using photovoltaic: Status and technological review," *Renewable and Sustainable Energy Reviews, vol. 54*, pp. 34-47, 2016.

[5] Chandra Mouli G.R., Bauer, P. and Zeman, M., "System design for a solar powered electric vehicle charging station for workplaces," *Applied Energy, Vol. 168,* pp. 434-443, 2016.

[6] Ma, T.,and Mohammed, O.A., "Optimal charging of plug-in electric vehicles for a car-park infrastructure," *IEEE Transactions on Industry Applications, vol. 50 (4),* pp. 2323-2330, 2014.

[7] Chen, Q., Wang, F., Hodge, B.-M., Zhang, J., Li, Z., Shafie-Khah, M. and Catalao, J.P.S., "Dynamic Price Vector Formation Model-Based Automatic Demand Response Strategy for PV-Assisted EV Charging Stations," *IEEE Transactions on Smart Grid, vol. 8 (6)*, pp. 2903-2915, 2017.

[8] Ito, A., Kawashima, A., Suzuki, T., Inagaki, S., Yamaguchi, T. and Zhou, Z., "Model Predictive Charging Control of In-Vehicle Batteries for Home Energy Management Based on Vehicle State Prediction," *IEEE Transactions on Control Systems Technology, vol. 26 (1),* pp. 51-64, 2018.

[9] Tushar, M.H.K., Assi, C., Maier, M. and Uddin, M.F., "Smart microgrids: Optimal joint scheduling for electric vehicles and home appliances," *IEEE Transactions on Smart Grid, vol. 5 (1),* pp. 239-250, 2014.

[10] Uddin, K., Dubarry, M. and Glick, M.B., "The viability of vehicle-to-grid operations from a battery technology and policy perspective," *Energy Policy, vol. 113,* pp. 342-347, 2018.

[11]   Bhatti, A.B., Salam, Z., Aziz, M., and Yee, K.P., "A critical review of electric vehicle charging using solar photovoltaic," *International Journal of Energy Research, vol. 40(4)*, pp. 439-461, 2016.

[12]   Liu, N., Chen, Q., Liu, J., Lu, X., Li, P., Lei, J., and Zhang, J., "A heuristic operation strategy for commercial building microgrids containing EVs and PV system," *IEEE Transactions on Industrial Electronics, vol. 62(4),* pp. 2560-2570, 2015.

[13]   Ma, T., and Mohammed. O. A., "Optimal charging of plug-in electric vehicles for a car-park infrastructure," *IEEE Transactions on Industry Applications, vol 50(4), pp. 2323-2330*, 2014.

[14]   Goldmark, A., "NYC Mayor Wants 10,000 New Electric Vehicle Charging Spaces," WNYC, 2013. [Online]. Available: http://www.wnyc.org/story/285133-nyc-mayor-wants-10000-new-electric-vehicle-charging-spaces.

[15]   Bonges, H.A., and Lusk, A.C., "Addressing electric vehicle (EV) sales and range anxiety through parking layout, policy and regulation," *Transportation Research Part A: Policy and Practice, vol. 83, pp. 63-73,* 2016.

[16]   Yilmaz, M., and Krein, P.T., "Review of battery charger topologies, charging power levels, and infrastructure for plug-in electric and hybrid vehicles." *IEEE Transactions on Power Electronics, vol. 28(5), pp. 2151-2169,* 2013.

[17]   Kanchev, H., Lu, D., Colas, F., Lazarov, V. and Francois, B., "Energy Management and Operational Planning of a Microgrid With a PV-Based Active Generator for Smart Grid Applications," *IEEE Transactions on Industrial Electronics, vol. 58 (10),* pp. 4583 – 4592, 2011.

[18]   Jian, L., Zhu, X., Shao, Z., Niu, S.,and Chan, C.C., "A scenario of vehicle-to-grid implementation and its double-layer optimal charging strategy for minimizing load variance within regional smart grids," *Energy Conversion and Management, vol. 78,* pp. 508-517, 2014.

[19]   Wu, X., Hu, X., Moura, S., Yin, X. and Pickert, V., "Stochastic control of smart home energy management with plug-in electric vehicle battery energy storage and photovoltaic array," *Journal of Power Sources, vol. 333,* pp. 203-212, 2016.

[20]   Golshannavaz, S., "Cooperation of electric vehicle and energy storage in reactive power compensation: An optimal home energy management system considering PV presence," *Sustainable Cities and Society, vol. 39,* pp. 317-325, 2018.

[21]   Melhem, F.Y., Grunder, O., Hammoudan, Z., and Moubayed, N., Optimization and Energy Management in Smart Home Considering Photovoltaic, Wind, and Battery

Storage System With Integration of Electric Vehicles, *Canadian Journal of Electrical and Computer Engineering, vol, 40 (2)*, pp. 128-138, 2017.

[22]   Yoshida, A., Yoshikawa, J., Fujimoto, Y., Amano, Y., and Hayashi, Y., "Stochastic receding horizon control minimizing mean-variance with demand forecasting for home EMSs," *Energy and Buildings, vol. 158,* pp. 1632-1639. 2018.

[23]   Gazafroudi, A.S., Pinto, T., Prieto-Castrillo, F., Prieto, J., Corchado, J.M., Jozi, A., Vale, Z. and Venayagamoorthy, G.K, "Organization-based Multi-Agent structure of the Smart Home Electricity System," *Proceedings, 2017 IEEE Congress on Evolutionary Computation,* Donostia-San Sebastian, Spain, pp. 1327-1334., 2017.

[24]   Petrollese, M., Valverde, L., Cocco, D., Cau, G. and Guerra, J., "Real-time integration of optimal generation scheduling with MPC for the energy management of a renewable hydrogen-based microgrid," *Applied Energy, vol. 166*, pp. 96-106, 2016.

[25]   Zhao, Y., Chen, Y. and Keel, B., " Optimal Scheduling of Home Energy Management System with Plug-in Electric Vehicles using Model Predictive Control," *Proceedings of the ASME 2018 Dynamic Systems and Control Conference*, Atlanta, GA, 2018.

[26]   Munkhammar, J., Widén, J. and Rydén, J., "On a probability distribution model combining household power consumption, electric vehicle home-charging and photovoltaic power production," *Applied Energy, vol. 142,* pp. 135-143, 2015.

[27]   Van Der Meer, D., Chandra Mouli, G., Morales-Espana, G., Ramirez Elizondo, L. and Bauer, P., "Energy Management System with PV Power Forecast to Optimally Charge EVs at the Workplace," *IEEE Transactions on Industrial Informatics, vol.14 (1),* pp. 311-320, 2016.

[28]   Texas Instruments website, 2018, Piccolo-based Solar Explorer Development Kit [Online], Available: http://www.ti.com/tool/TMDSSOLARPEXPKIT#buy.

[29]   Texas Instruments website, 2018, TMS320F28035, [Online], Available: http://www.ti.com/product/TMS320F28035.

[30]   Arduino website, 2018, Arduino Uno, [Online], Available: https://store.arduino.cc/usa/arduino-uno-rev3.

[31]   Implementing Photovoltaic Inverter System using C2000 Microcontrollers on Solar Explorer Kit, [Online], Available: https://e2e.ti.com/cfs-file/__key/communityserver-discussions-components-files/171/PVInverter_5F00_F2803x.pdf.

[32]   implementing photovoltaic battery charging system using c2000 microcontrollers on solar explorer kit, [Online], Available: http://e2e.ti.com/cfs-

file/__key/communityserver-discussions-components-files/171/1665.PV_5F00_BatteryCharging_5F00_F2803x_5F00_0_5F00_1.pdf.

[33]   Texas Instruments website, 2018, controlSUITE Software Suite, [Online], Available: http://www.ti.com/tool/CONTROLSUITE.

[34]   Texas Instruments website, 2018, Code Composer Studio (CCS) Integrated Development Environment (IDE), [Online], Available: http://www.ti.com/tool/CCSTUDIO.

[35]   Kwon, W., H. and Han, S., H., 2005, Receding Horizon Control, Springer-Verlag London, 1st Edition.

[36]   Ruchika, N.R., "Model predictive control: History and development," *International Journal of Engineering Trends and Technology (IJETT), vol. 4(6),* pp.2600-2602, 2013.

[37]   Bemporad, A. and Morari, M., "Control of systems integrating logic, dynamics, and constraints," *Automatica, vol. 35 (3),* pp. 407-427, 1999.

[38]   OpenEI website, 2018, Commercial and Residential Hourly Load Profiles for all TMY3 Locations in the United States [Online], Available: https://openei.org/datasets/dataset/commercial-and-residential-hourly-load-profiles-for-all-tmy3-locations-in-the-united-states.

[39]   Tesla website, 2018, Model S, [Online], Available: https://www.tesla.com/model-s.

[40]   SRP website, 2018, Electric Vehicle Price Plan [Online], Available: https://www.srpnet.com/prices/home/electricvehicle.aspx.

[41]   SRP website, 2018, Customer Generation Price Plan [Online], Available: https://www.srpnet.com/prices/home/customergenerated.aspx.